Taylor & Francis
Taylor & Francis Group

Corrosion Engineering, Science and Technology

The International Journal of Corrosion Processes and Corrosion Control

ISSN: (Print) (Online) Journal homepage: https://www.tandfonline.com/loi/ycst20

# Corrosion behaviour of the 2098-T351 Al–Cu–Li alloy after different surface treatments

**Wanessa das Graças Barboza, Mariana Xavier Milagre, Uyime Donatus, Caruline de Souza Carvalho Machado, Oscar Mauricio Prada Ramirez, João Victor de Sousa Araujo, Rejane Maria Pereira da Silva & Isolda Costa**

**To cite this article:** Wanessa das Graças Barboza, Mariana Xavier Milagre, Uyime Donatus, Caruline de Souza Carvalho Machado, Oscar Mauricio Prada Ramirez, João Victor de Sousa Araujo, Rejane Maria Pereira da Silva & Isolda Costa (2022): Corrosion behaviour of the 2098-T351 Al–Cu–Li alloy after different surface treatments, Corrosion Engineering, Science and Technology, DOI: 10.1080/1478422X.2022.2054915

**To link to this article:** https://doi.org/10.1080/1478422X.2022.2054915

Published online: 29 Mar 2022.

CORROSION ENGINEERING, SCIENCE AND TECHNOLOGY
https://doi.org/10.1080/1478422X.2022.2054915

I·M3 Institute of Materials, Minerals & Mining
Taylor & Francis Taylor & Francis Group

RESEARCH ARTICLE



# Corrosion behaviour of the 2098-T351 Al–Cu–Li alloy after different surface treatments

Wanessa das Graças Barboza[a], Mariana Xavier Milagre [a], Uyime Donatus [a], Caruline de Souza Carvalho Machado [b], Oscar Mauricio Prada Ramirez [b], João Victor de Sousa Araujo [a], Rejane Maria Pereira da Silva [a] and Isolda Costa [a]

[a]Centro de Ciência e Tecnologia dos Materiais, Instituto de Pesquisas Energéticas e Nucleares, IPEN/CNEN, São Paulo, Brazil; [b]Departamento de Engenharia Metalúrgica e de Materiais, Universidade de São Paulo, PMT/USP São Paulo, Brazil

**ABSTRACT**

The effect of different surface treatments on the corrosion resistance of the AA2098 Al–Cu–Li alloy has been investigated. Surface characterization was performed using 3D optical profilometry, energy dispersive X-ray spectroscopy and scanning electron microscopy. The corrosion resistance of the 2098 alloy after the surface treatments was investigated in 0.1 mol $L^{-1}$ NaCl solution by electrochemical techniques and microscopy. Corrosion results showed that the untreated and the chemically etched surfaces were more active than the mechanically abraded and mechanically polished surfaces owing to differences in the nature of the native oxides formed after the surface treatments. Corrosion rate and mode were also affected by how close the exposed surface was to the mid-thickness region of the AA2098-T351 plate relative to the actual top surface (before polishing). This is associated with the variation in the volume fraction and distribution of the T1 phase as the mid-thickness region of the AA2098-T351 plate is approached.

**ARTICLE HISTORY**
Received 4 January 2022
Accepted 12 March 2022

**KEYWORDS**
Al alloys; localized corrosion; surface characterization

## Introduction

The Al–Cu–Li alloys have been reported as potential substitutes for conventional Al-alloys from the 2xxx series in the aircraft industry owing to their excellent mechanical and fatigue resistance and lower density compared to the conventional alloys, which allow reduction in the aircraft weight and, consequently, a decrease in fuel consumption [1–3].

The 2098 is a 3rd generation Al–Cu–Li alloy. For this alloy, the phase responsible for its strengthening is the T1 ($Al_2CuLi$) phase [4–7]. The T1 phase is a metastable strengthening phase characterized by a hexagonal platelet structure [8–11]. According to a previous work [12], four variants of this phase was identified in the 2098 alloy in the [110] zone axis diffraction pattern (two variants producing superlattice spots at 1/3 and 2/3 of ⟨220⟩ and the other two variants appearing as continuous streaks along ⟨111⟩). Also, at the [112] zone axis, some superlattice spots and continuous streaks in ⟨111⟩ direction, were observed. Despite its contribution to the excellent mechanical properties of the Al–Cu–Li alloys, this phase has been reported as harmful to corrosion resistance [13–15].

The corrosion degradation of the Al–Cu–Li alloys starts with the selective dissolution of the Li present in the T1 phase [16]. As previously reported [17], since Li is highly reactive, its presence in the T1 phase makes this phase anodic in relation to the Al-alloy matrix. Thus, the T1 phase is easily dissolved, when in contact with aggressive media, and, consequently, the remaining phase becomes Cu-enriched and cathodic relative to the matrix. The T1 phase precipitates mainly at dislocations, thus thermomechanical processes that affect dislocation density and distribution also influence the corrosion behaviour of T1 phase-containing alloys [18]. According to Milagre et al. [19], the 2098-T351 intragranular corrosion susceptibility is related to the high density of T1 precipitates inside its grains. However, Lei et al. [20] observed preferential corrosion at the grain boundaries of the 2098-T851 alloy, and intergranular corrosion propagation. Moreover, depending on the aggressiveness of the environment, exfoliation can also be observed in this kind of alloys [21].

It is important to highlight the fact that the nature of the exposed surface of the alloy (dependent on the treatment before exposure to the corrosive environment) significantly influences the corrosion mode and rates in wrought Al alloys including the Al–Cu–Li alloys. This is partly owing to the presence of a near-surface deformed layer (NSDL) developed during the manufacturing of the alloys. The NSDL has different microstructural and chemical features in relation to the bulk. These differences influence the corrosion behaviour of the Al-alloys. Etching and polishing remove this layer, but they produce new surfaces with different corrosion characteristics. In previous works [22,23], the electrochemical activity of the polished AA2098-T351 surface was compared with that of the original surface of the same alloy with NSDL and the results showed great differences between the two types of surfaces [22]. However, works involving the comparison between surface polishing (to different depths from the top surface), grinding and etching (pickling) of the AA2098-T351 alloy have not been reported in the past. All these surface finishing processes are industrially relevant and the results from the investigation of the corrosion behaviour of the surfaces produced by these finishing processes will further the understanding of corrosion mechanisms and mitigation methods for Al–Cu–Li alloys.

**CONTACT** Mariana Xavier Milagre marianamilagre@yahoo.com.br IPEN/CNEN-SP (CCTM), Av. Professor Lineu Prestes, 2242, São Paulo, SP, Brazil

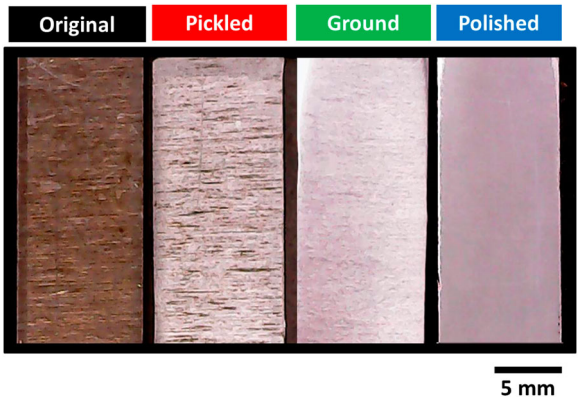


**Figure 1.** Surface finishing after the pretreatments of the 2098-T351 Al–Cu–Li alloy investigated in this study.

Thus, this work has focused on investigating the effect of different surface finishing processes on the corrosion behaviour of the AA2098-T351 Al–Cu–Li alloy. Corrosion assessment after polishing to different depths, grinding, and pickling in comparison to the original surface without prior treatment has been carried. The alloy surface was characterized after each surface treatment and compared with the original rolled surface using scanning electron microscopy (SEM), energy dispersive X-ray spectroscopy (EDX) and 3D profilometry. The electrochemical behaviour was monitored in 0.1 mol $L^{-1}$ of NaCl and the electrochemical activity related to each condition was analyzed in an oxidizing media by local electrochemical impedance spectroscopy (LEIS).

## Experimental

### Material

The 2098-T351 used in this study was received in a plate shape with a thickness of 3 mm. The alloy composition obtained by inductively coupled plasma optical emission spectrometry (ICP-OES) is as follow: Cu 3.4 wt-%, Li 1.0 wt-%, Mg 0.3 wt-%, Ag 0.3 wt-%, Zr 0.4 wt-%, Fe 0.04 wt-%, Si 0.05 wt-%, Zn 0.02 wt-% and, Mn 0.003 wt-%.

### Surface finishing

The effect of five different surface finishing processes was analyzed in this work, Figure 1. The untreated sample presents a near surface deformed layer (NSDL) at the surface owing to the fabrication process. Alkaline attack step was carried out in a solution composed of 10% NaOH at 40°C for 30 s, and then rinsed for 3 min in deionized water followed by neutralization in a chromate-free commercial acidic solution, TURCO SMUTT-GO, at room temperature for 15 s, before a final rinse in deionized water for 3 min. Ground samples were metallographically prepared by mechanical grinding with SiC papers (#500, #800, #1200, #2500, #4000). After grinding, the samples were polished with diamond suspensions of 3 and 1 µm.

### Surface examination

The microstructure of the 2098-T351 Al–Cu–Li was examined by optical microscopy after etching in a solution composed of 3% HF, 25% $HNO_3$ in 100 mL of deionized water.

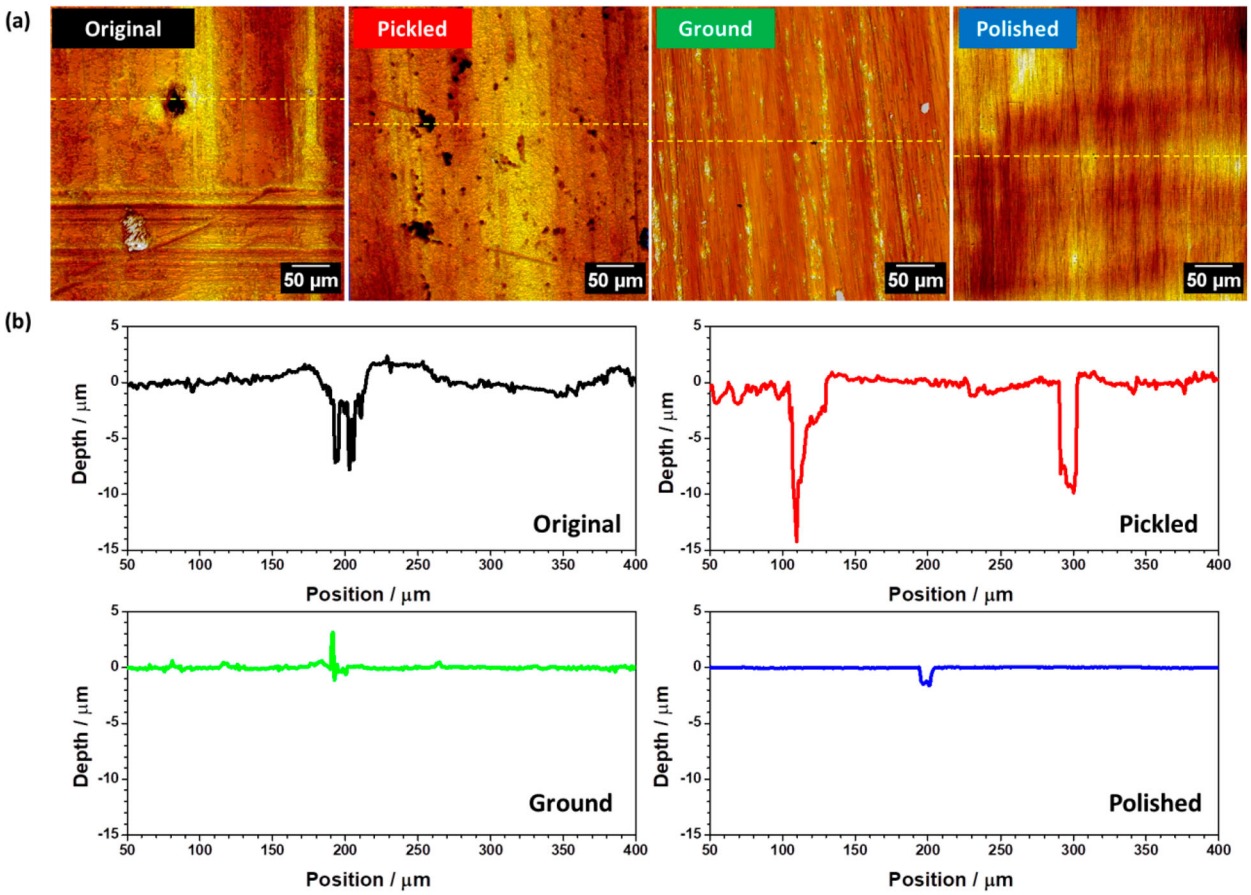


**Figure 2.** (a) 3D profilometry images of the different surface finish. (b) Height profiles related to the regions with the yellow dashed lines in (a).

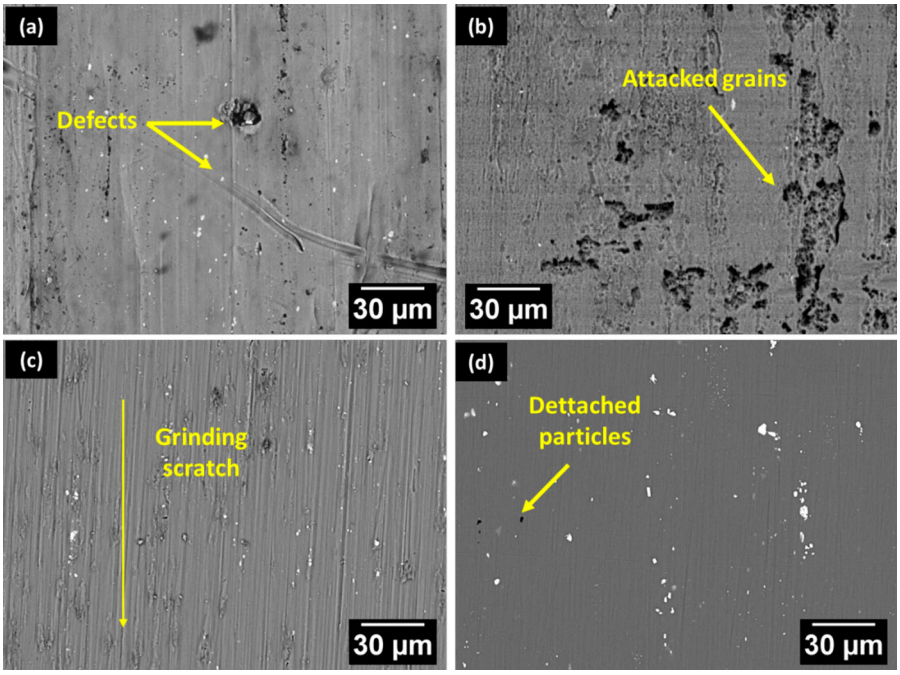


**Figure 3.** SEM images of the surface of the 2098-T351 alloy with different surface finish: (a) original; (b) pickled; (c) ground; and (d) polished surfaces.

SEM images were acquired using a Hitachi TM 3000 microscope equipped with an EDX detector. The electron microscope was operated using an incident beam of 15 kV. An ZYGO's ZeGage™ 3D optical profilometer was also used.

### *Immersion test*

Samples of the 2098-T351 Al–Cu–Li alloy were exposed to 0.1 mol $L^{-1}$ of NaCl for 48 h at 22 ± 2°C and the development of corrosion was monitored by optical microscopy. The exposed area was 0.09 $cm^2$.

### *Electrochemical characterization*

Potentiodynamic polarization tests were performed using an Autolab PGSTAT potentiostat controlled by NOVA 2.1 software. All measurements were performed at 22 ± 2°C in naturally aerated 0.1 mol $L^{-1}$ NaCl solution using a three-electrode set-up. An Ag/AgCl/KCl(sat) electrode was used as the reference electrode, a platinum wire as the counter electrode, and the Al alloy as the working electrode. The area of the working electrode exposed to the test solution was 0.09 $cm^2$. Polarization curves were obtained at a scan rate of 1 mV/s, from OCP to 1 V.

## Results and discussion

### *Surface finishing characterization*

Figure 2, shows a 3D profilometer analysis corresponding to each surface finishing studied in this work. As observed by the height profiles (Figure 2(b)) the original and the pickled samples exhibited higher roughness profiles compared to the ground and polished samples.

Although the roughness profiles of the surfaces of the original and pickled samples were similar, both surfaces showed different morphologies, as can be seen from the

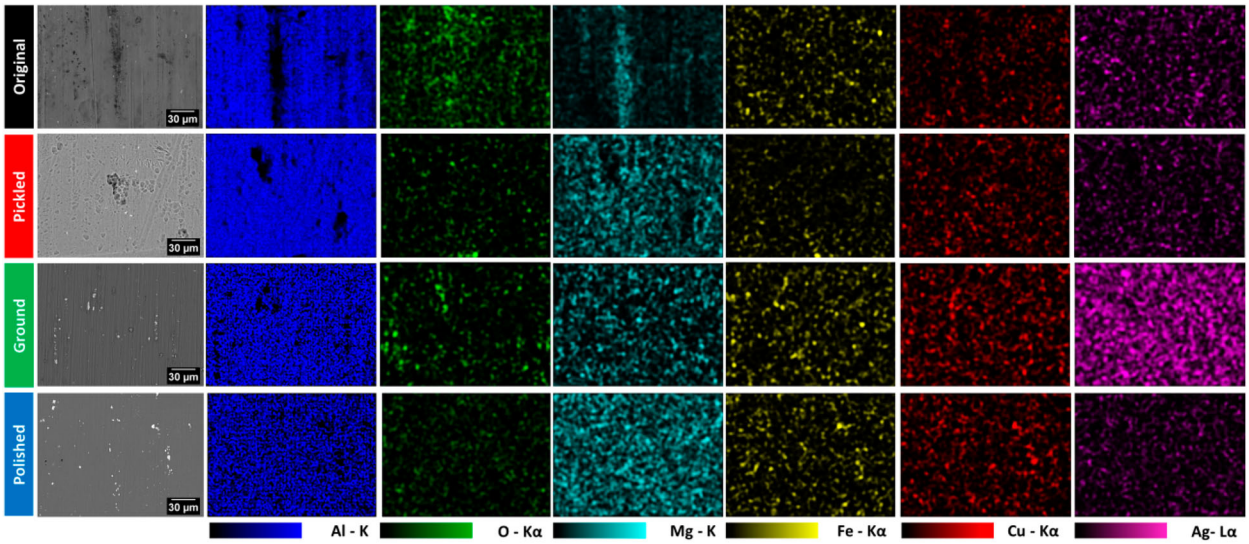


**Figure 4.** EDX maps of the surface of the 2098-T351 alloy with different surface finish.

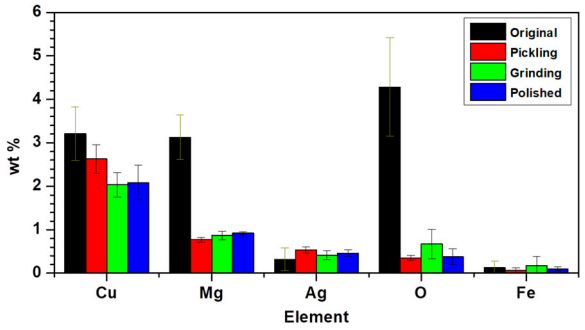


**Figure 5.** Average weight per centage of the composition of the matrix of the 2098-T351 Al–Cu–Li alloy after different surface finishing – obtained by EDX.

SEM images in Figure 3. For the original samples, the deepest penetrations are associated with defects produced by the manufacturing process of the alloy (Figure 3(a)), whereas those of the pickled samples are owing to the chemical attack of the alloy in NaOH (Figure 3(b)). The peaks and valleys in the ground samples are associated with the scratches (Figure 3(c)) owing to abrasion with the SiC paper, whereas the depressions in the polished sample are related to the detached particles removed during polishing (Figure 3(d)).

The original Al-alloy presents a near-surface deformed layer (NSDL) which is enriched in Mg and Mg oxides. This layer is removed when the alloy is chemically attacked, ground or polished, as can be observed from the EDX maps, Figure 4.

Besides the higher signals of Mg observed by EDX maps for the original surface, Figure 5 showed higher Cu signals content in the matrix of the original and pickled samples compared with the ground and polished surfaces. The ground and polished surfaces showed a more homogeneous chemical composition.

Despite the removal of the Mg bands by pickling, grinding and polishing, cross-sectional images of the samples showed differences in grain sizes near the treated surfaces, Figure 6. Coarsened grains were observed near to the top surface layer, and this layer thickness is reduced depending on surface finishing. Tens of micrometres were removed by pickling, whereas hundreds of micrometres by grinding and polishing. However, coarsened grains were still observed in the cross-section of the polished sample. For this reason, to evaluate the effect of this layer on the corrosion behaviour of the polished samples, the two different thicknesses of the top surface of the polished samples were analyzed.

## Corrosion behaviour

Figure 7 shows the evolution of the different surfaces of the AA2098-T351 alloy in the NaCl solution used in this study. The figure shows that all the surfaces are active in the immersion solution from the first minutes of immersion. Corrosion propagation on the original samples are related to the Mg enriched bands. The attack extended to the rest of the surface after the consumption of the magnesium-rich bands. The great volume of corrosion products even in the first hours of immersion shows how active this surface is. After 8 h of immersion, the corrosion product had spread all over the exposed area and its volume increased with time until the test was stopped. Corrosion propagation on the pickled sample was associated with the pre-attacked grains, as shown in Figure 3. Small pits were observed for the ground samples, while the polished samples showed severe localized corrosion (SLC).

## Electrochemical activity

Anodic polarization curves of the AA2098-T351 alloy with the different surface finish were obtained after 30 min of immersion in 0.1 mol $L^{-1}$ of NaCl solution, Figure 8(a). The polarization curves show that the original condition presented the highest anodic activities compared with the other conditions tested and no pseudo-passive behaviour was

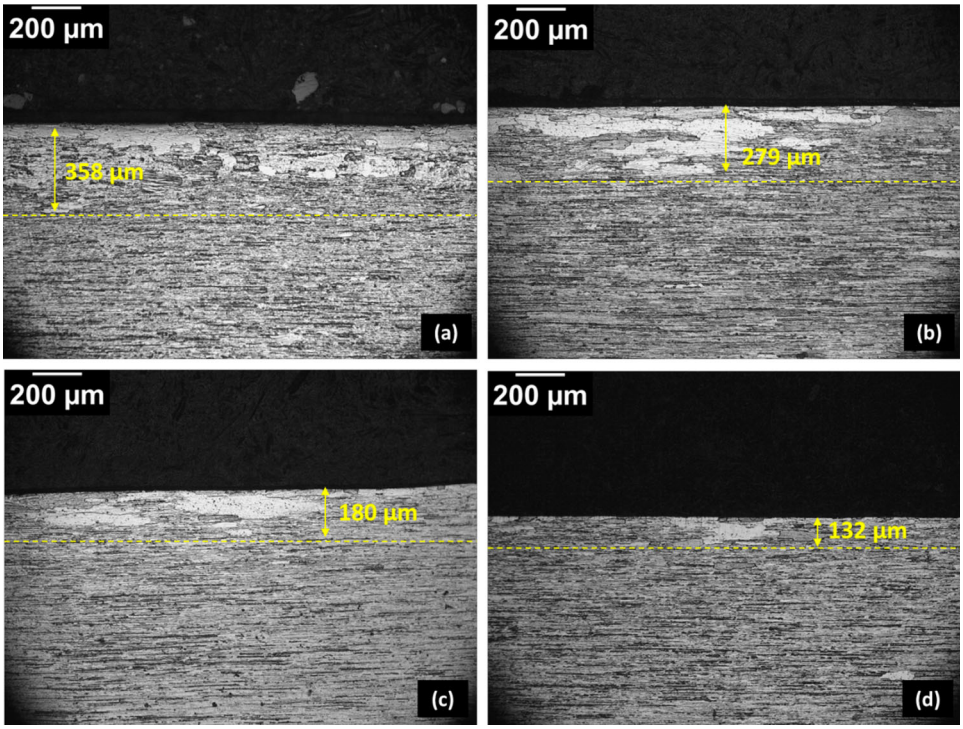


**Figure 6.** Optical microscopy of the cross-section of the 2098-T351 alloy with different surface finish. (a) original; (b) pickled; (c) ground; (d) polished surface.

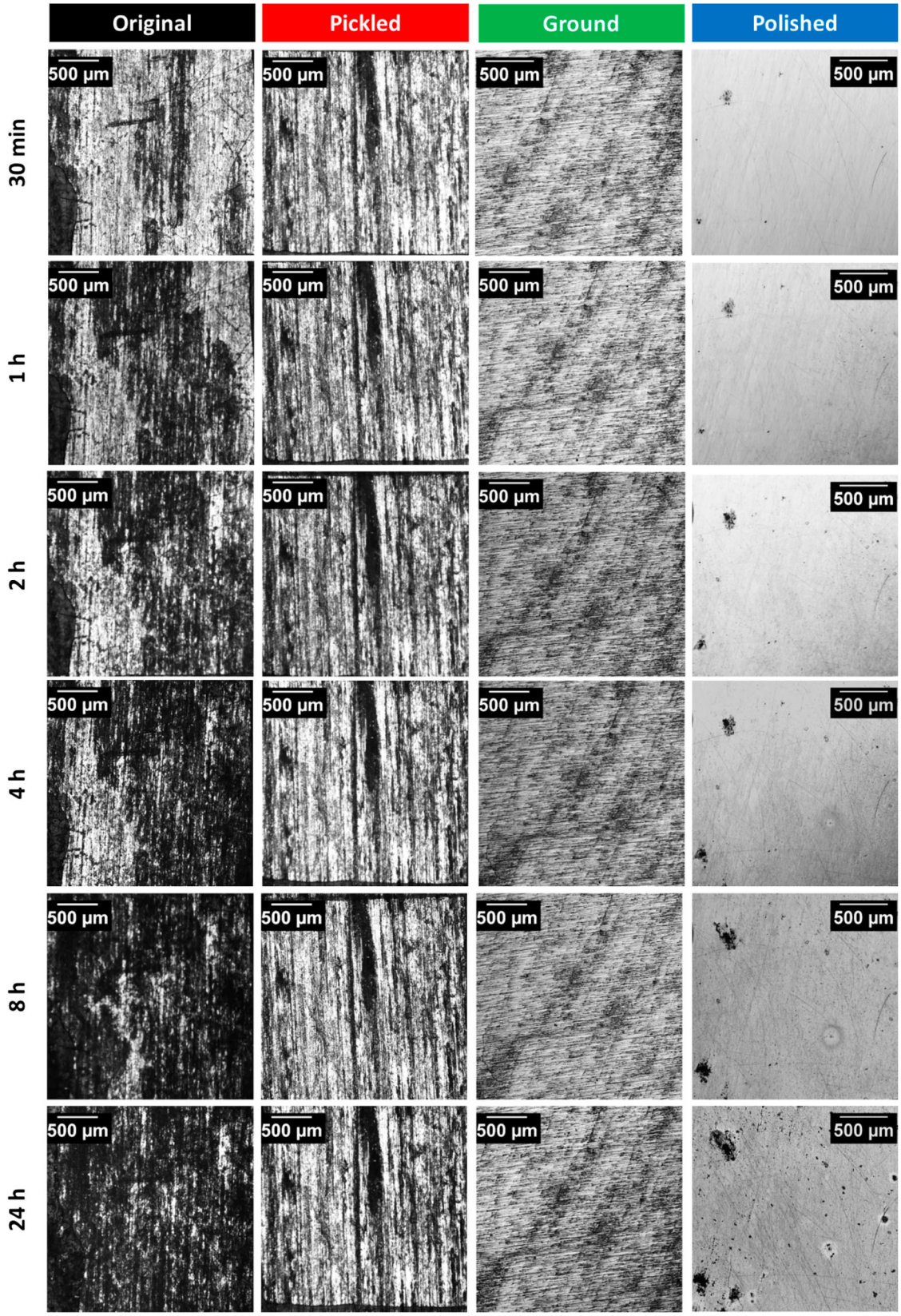


**Figure 7.** Evolution of the differently treated surfaces of the 2098-T351 alloy in 0.1 mol $L^{-1}$ NaCl.

observed for this condition. This was followed by the pickled sample which also showed no passivation but a slight pseudo-passive behaviour, Figure 8(b). The current density values of the ground and polished samples were significantly lower compared with the original and pickled samples. The polished sample presented the lowest current density values but the values were close to those of the ground sample and the breakdown potential for both samples was similar, Figure 8(b). Also, unlike the original and pickled samples, the ground and polished samples presented distinct pseudo-passive ranges with similar breakdown potentials.

The corrosion features observed from the optical micrographs of the samples after polarization tests are in agreement with the polarization results, Figure 8(c). The corroded area of the original sample was the largest. For

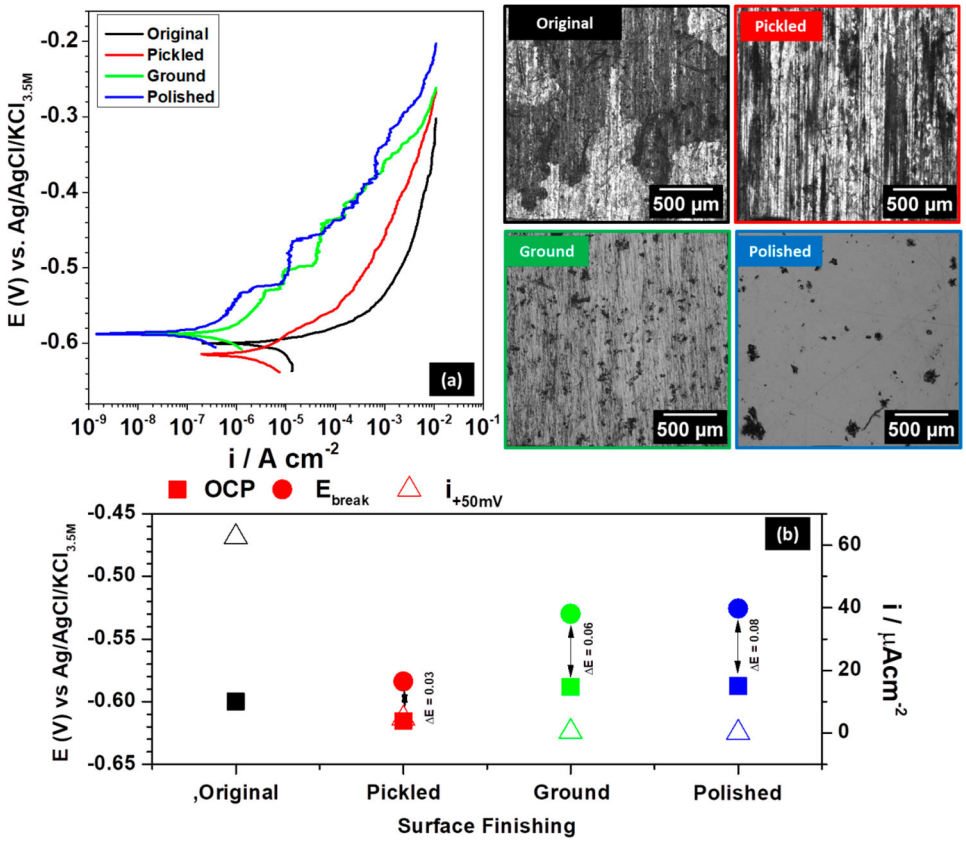


**Figure 8.** (a) Anodic polarization curves for the 2098-T31 Al–Cu–Li alloy with different surface finish after 30 min of immersion in 0.1 mol $L^{-1}$ NaCl solution. (b) Differences between the open circuit potentials (OCP) and the breakdown potentials beyond pseudo-passivity ($E_{break}$). (c) Optical microscopy of the tested surfaces.

the pickled sample, the attack was favoured in the grains, similarly to the effect of the surface treatment as observed in Figure 3. Pit density was higher for the ground sample compared to the polished one explaining the higher current densities for the ground surface.

The results of the local electrochemical behaviour of each surface condition analyzed by local electrochemical impedance spectroscopy (LEIS) measurements are shown in Figure 9. The LEIS results are in agreement with the previously shown results. All the surfaces were active from the first minutes of immersion. The original sample surface presented the highest admittance values for the entire duration of the test. For the Ground and Polished conditions, the regions of higher admittance were related to the SLC sites and variations in these values with time were related to deposition of corrosion products over the surfaces. The Polished and Ground samples showed similar admittance values, corroborating the results of the polarization curves.

Surface examination and EDX analysis of the attacked regions during LEIS tests are shown in, Figure 10. Cu and Ag redeposition were observed near the corroded sites, mainly on the polished surfaces. Fe was associated with the micrometric particles for all analyzed surface finishing. Mg oxide was associated with the deformation bands for the original condition.

Figure 11 shows the 3D profilometry analysis of the surfaces exposed to 0.005 mol $L^{-1}$ NaCl solution during the LEIS test. The pits formed by exposure to the LEIS test solution showed smaller diameters, Figure 11(a), but deep penetration. This result explains the higher admittance values observed in Figure 9. The pickled samples were associated with high admittances (with values only lower than that of the original samples) and this result also explains the high pit depths for this condition, Figure 11(b). For the Ground and Polished samples, the 'mouth of the pits' were comparatively large, Figure 11(a), but shallow, Figure 11(b). This can be associated with the lower kinetics of the reactions for these two surface conditions as was shown in Figure 8. The improved corrosion resistance of the Polished surface is related to the enhancement of natural oxide film formation over this surface. Despite the presence of SLC sites, areas with preserved oxide film were still present over this surface reducing the global current density measured. On the other hand, the presence of Mg and Cu on the surfaces of the original and pickled samples, respectively, were responsible for the higher corrosion kinetics for these conditions.

### *Effect of near-surface grain coarsening*

In order to evaluate the effect of the layer with coarsened grains at the near-surface (as observed in Figure 6) on the corrosion behaviour of the Polished samples, the corrosion test was also performed by comparing two different levels of polishing depths (labelled as Polished and Mid-thickness). The Polished sample (Figure 6(d)) represents the condition where the coarsened-grain layer is still observed after polishing while the Mid-thickness sample was prepared in order to remove this layer and it represents the surface of the middle portion of the plate. Figure 12 showed the evolution of the corrosion features on the Mid-thickness samples immersed in 0.1 mol $L^{-1}$ NaCl. According to the results, higher corrosion activities were observed for this condition, when compared with the Polished sample presented in Figure 7. These higher activities were associated with the great volume of

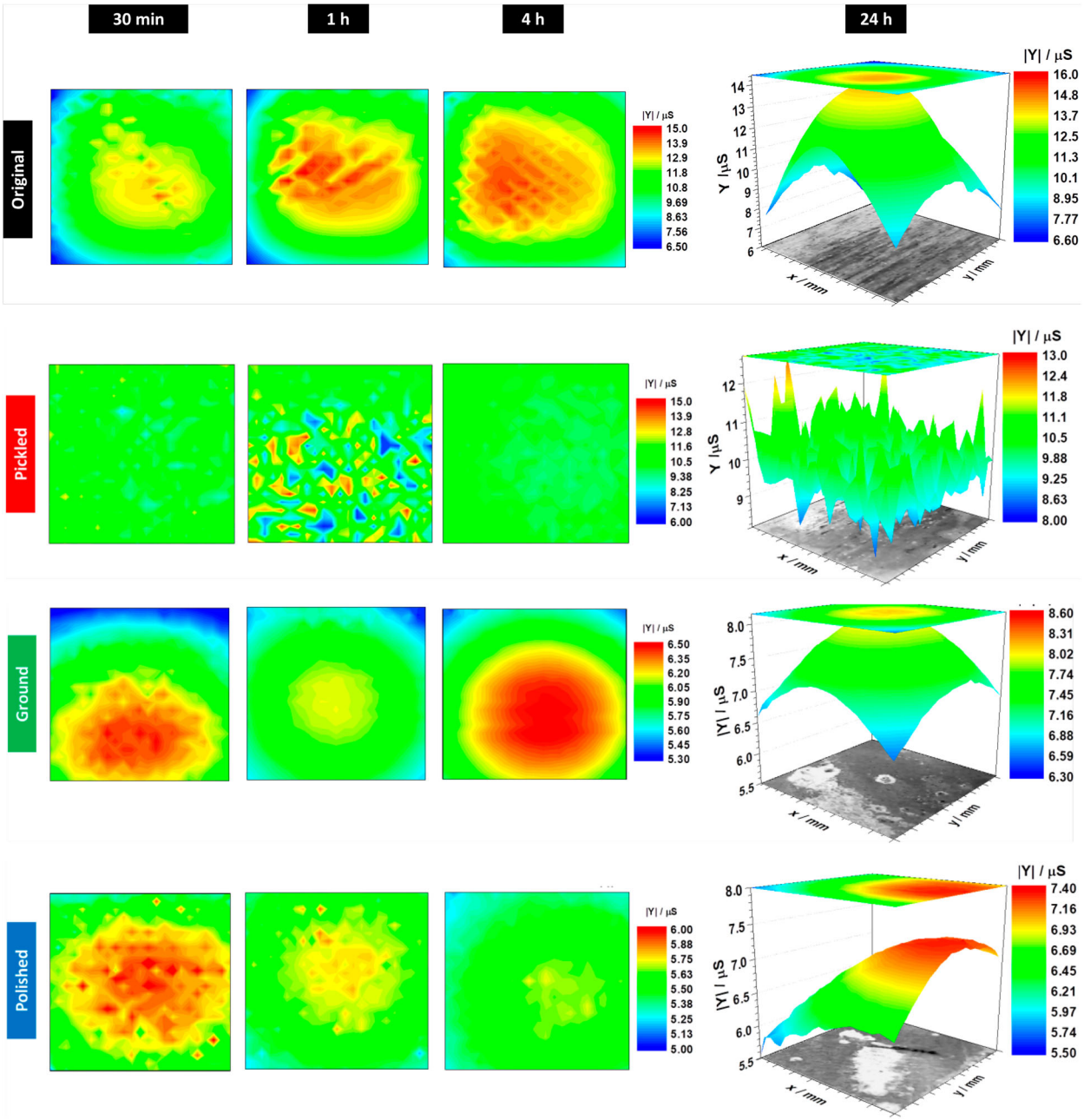


**Figure 9.** Local admittance of the 2098-T351 alloy with different surface finishing during immersion test in 0.005 mol $L^{-1}$ NaCl solution (acquisition frequency: 5 Hz).

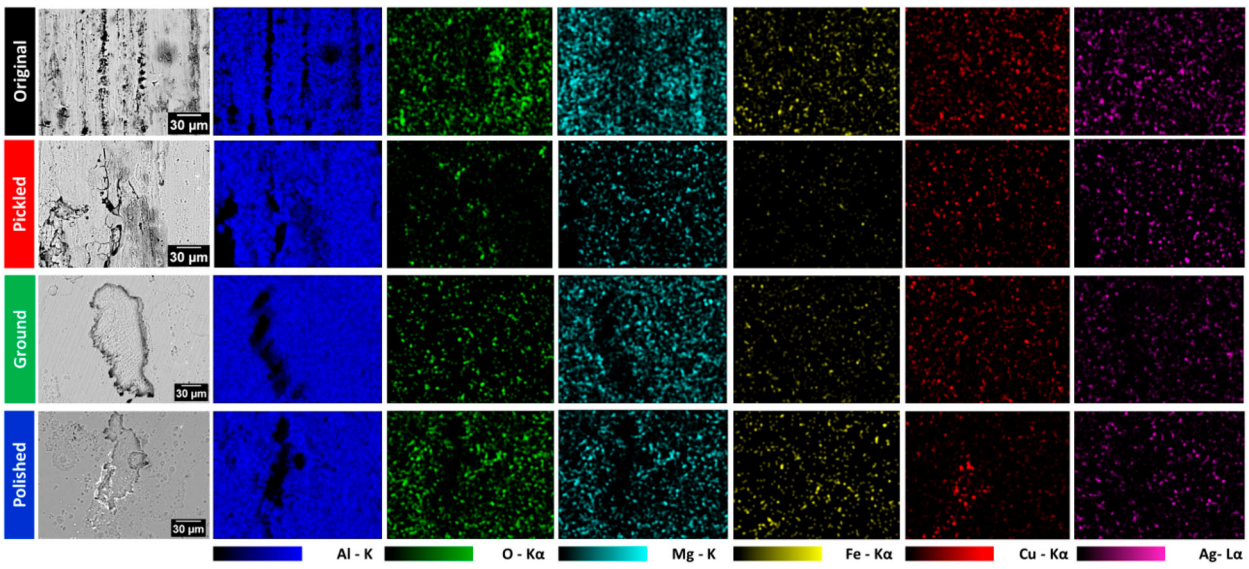


**Figure 10.** EDX maps of the surface of the 2098-T351 alloy with different surface finishing after immersion in NaCl for 24 h.

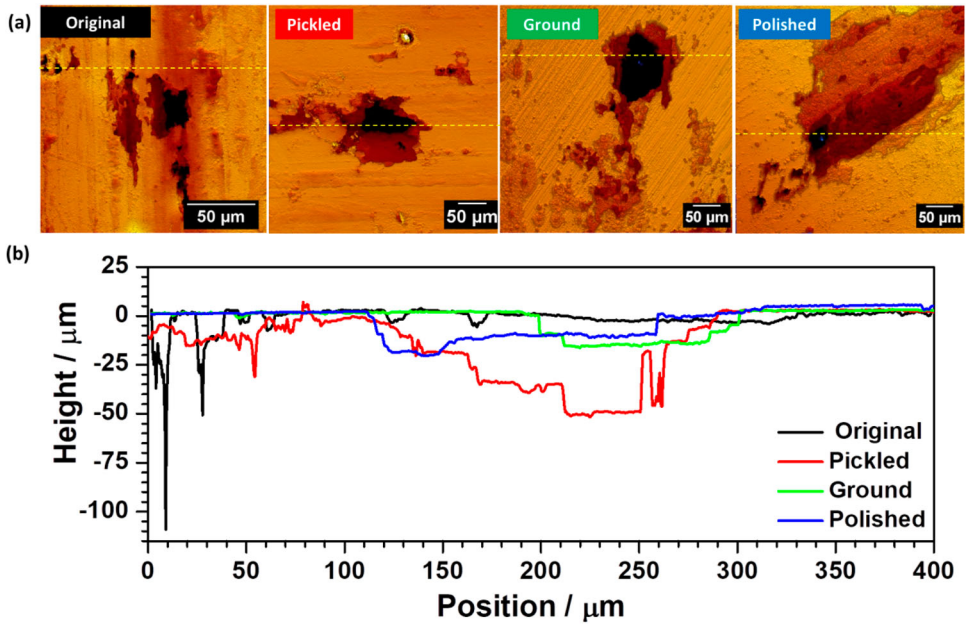


**Figure 11.** (a) 3D profilometry images of the different surface finishing after immersion in 0.005 mol $L^{-1}$ NaCl for 24 h. (b) Height profiles related to the yellow dashed lines in (a).

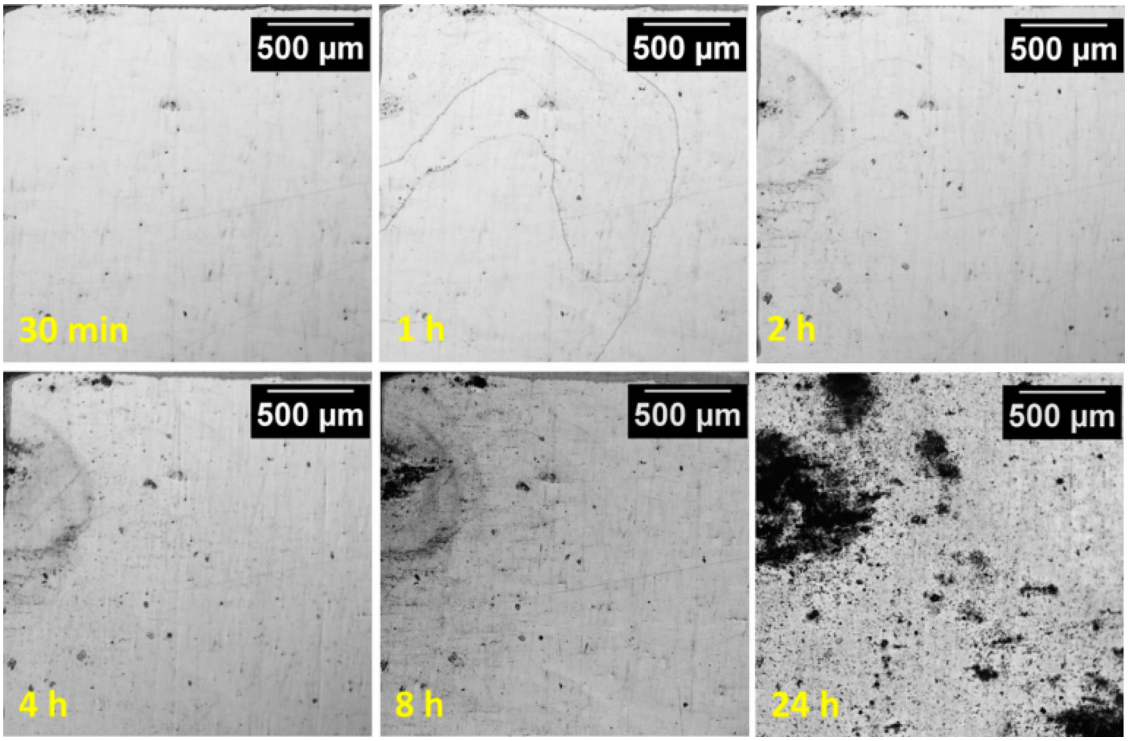


**Figure 12.** Evolution of the 2098-T351 top polished surface with 1.5 mm thickness exposed to 0.1 mol $L^{-1}$ NaCl for periods until 24 h.

corrosion products observed in the vicinity of the SLC regions.

Additionally, different propagation features were observed according to the alloy thickness, Figure 13. While intergranular attacks were observed on the surface of the Polished sample, the preferential corrosion propagation observed on the top surface of the Middle Plate sample was intragranular.

The electrochemical results are in agreement with the evolution of corrosion features on the surface of the samples, Figure 14. The anodic curves for the Mid-thickness sample were shifted more to the right (with higher anodic current densities) compared to the Polished sample as revealed in Figure 14a. Additionally, the optical images of the exposed surface after the test showed higher pit density for the Mid-thickness samples – Figure 14(b). The admittance values obtained were also lower for the Mid-thickness sample according to the LEIS maps in Figure 14(c).

Xu et al. [24] reported microstructural and crystallographic inhomogeneity in thick-sectioned Al–Li–Cu–Mg plates. According to the authors, strong crystallographic texture orientation at the mid-thickness and an increment in the volume fraction of intragranular T1 phase precipitates at the plate centre were observed. This explains the

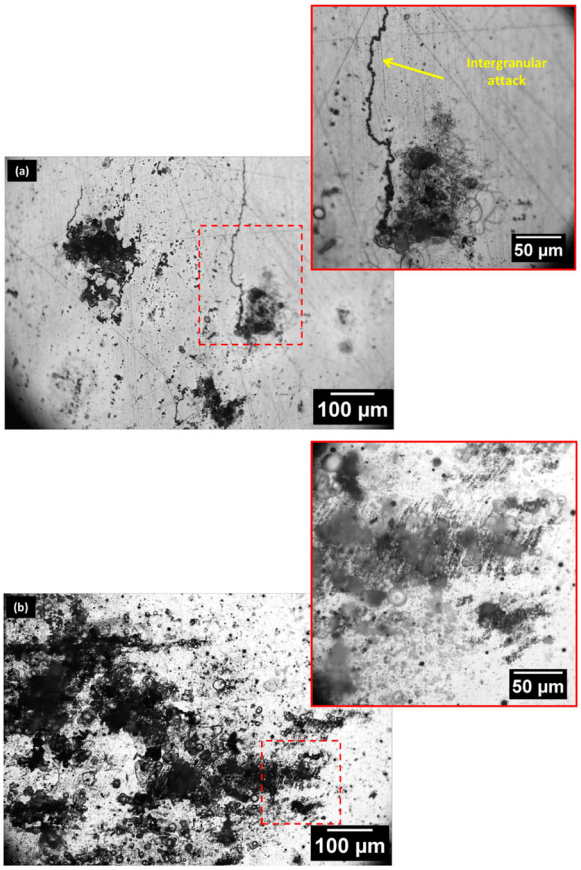


**Figure 13.** High magnification images of severe localized corrosion regions on the surface of polished 2098-T351 samples showing different corrosion features. (a) Polished 3.2 thk sample. (b) Polished 1.5 thk sample.

higher activity observed on the surface of the Mid-thickness sample when compared to the Polished sample. The higher pit density observed for the Mid-thickness sample and the predominance of intragranular attack observed in this condition is in accordance with the findings of Xu et al. These microstructural heterogeneities are a result of the variation of deformation strain and temperature. Lower cooling rate at the mid-thickness position has been reported to form a large amount of quench-induced T1 phases in a thick-section plate and the distribution of precipitates also varies according to the variation of deformation strain [25–27].

## Conclusions

The results of this study on the effect of surface treatments on the 2098-T351 Al–Cu–Li alloy led to the following conclusions:

1. The original samples showed the highest electrochemical activity, which was related to the presence of Mg bands – a characteristic of the near-surface-deformed layer.
2. Pickled samples presented high electrochemical activity resulting from preferential attacks inside the grains and Cu redeposition owing to etching-related Cu dissolution.
3. Ground and Polished surfaces showed the lowest electrochemical activities owing to improved oxide film formation.
4. Polished surfaces resulted in the lowest current densities compared to the Ground ones owing to slight improve-

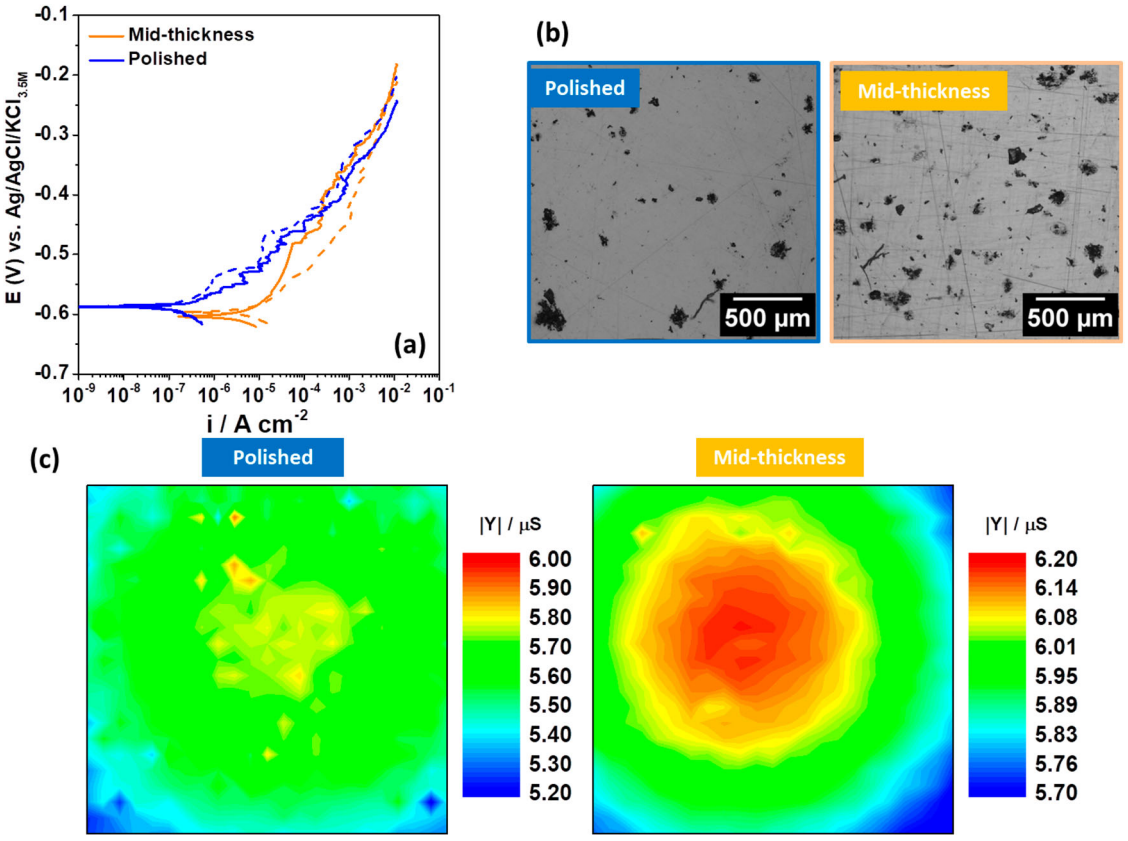


**Figure 14.** (a) Anodic polarization curves obtained for the Polished 2098-T351 and Mid-thickness samples in 0.1 mol $L^{-1}$ of NaCl solution. (b) Optical images of the polarized surfaces. (c) Local admittance maps obtained after 1 h of immersion in 0.005 mol $L^{-1}$ NaCl solution with an acquisition frequency of 5 Hz.

ment in the characteristics of the oxide film formed on the Polished surface.
5. Severe localized corrosion was not observed for the Ground surface under free corrosion potential conditions.
6. Corrosion activities were strongly linked with the depth level of the exposed polished surface relative to the unpolished original surface. The closer the tested surface is to the mid-thickness line of the plate the higher the corrosion rate owing to increasing volume fraction of T1 phase with depth. The mode of corrosion was also different with intragranular attack becoming predominant as the mid-thickness region is approached.

## Acknowledgements

The authors acknowledge CNPq-PIBIC for the grants of Wanessa G. Barboza and FAPESP for financial support (2013/12323-6) and the grant of R. Silva (Proc. 2018/06880-6). Acknowledgements are also owing to the Polytechnic School of São Paulo University (PMT/USP), Dr Hercilio G. de Melo, for the LEIS analysis and to Dr Antonello Astarita from the University of Naples for providing the 2098-T351 Al–Cu–Li alloy material.

## Disclosure statement

No potential conflict of interest was reported by the authors.

## Funding

This work was supported by Conselho Nacional de Desenvolvimento Científico e Tecnológico; Fundação de Amparo ã Pesquisa do Estado de São Paulo [grant number 2013/12323-6; 2018/06880-6].

## Data availability

The raw/processed data required to reproduce these findings cannot be shared at this time as the data also forms part of a continuing study.

## ORCID

*Mariana Xavier Milagre* http://orcid.org/0000-0003-2048-2863
*Uyime Donatus* http://orcid.org/0000-0001-8871-3571
*Caruline de Souza Carvalho Machado* http://orcid.org/0000-0003-4172-119X
*Oscar Mauricio Prada Ramirez* http://orcid.org/0000-0001-6904-8959
*João Victor de Sousa Araujo* http://orcid.org/0000-0001-6375-0480
*Rejane Maria Pereira da Silva* http://orcid.org/0000-0003-0081-8323
*Isolda Costa* http://orcid.org/0000-0002-4987-3334

## References

[1] Warner T. Recently-developed aluminium solutions for aerospace applications. Mater Sci Forum. 2006;519–521:1271–1278. doi:10.4028/www.scientific.net/MSF.519-521.1271.
[2] Wanhill RJH, Bray GH. Aerostructural design and its application to aluminum – lithium alloys. In: NE Prasad, A Gokhale, RJH Wanhill, editors. Alum. – Lithium Alloy. Process. Prop. Appl. Oxford: Elsevier Inc; 2014. p. 27–58. doi:10.1016/B978-0-12-401698-9.00002-1.
[3] Lequeu P, Smith KP, Daniélou A. Aluminium-copper-lithium alloy 2050 developed for medium to thick plate. J Mater Eng Perform. 2010;19:841–847. doi:10.1007/s11665-009-9554-z.
[4] fei Zhang S, dong Zeng W, hua Yang W, et al. Aging response of a Al-Cu-Li 2198 alloy. Mater Des. 2014;63:368–374. doi:10.1016/j.matdes.2014.04.063.
[5] Salem HG, Lyons JS. Effect of equal channel angular extrusion on the microstructure and superplasticity of an Al-Li alloy. J Mater Eng Perform. 2002;11:384–391. doi:10.1361/105994902770343908.
[6] Chen DL, Chaturvedi MC. Effects of welding and weld heat-affected zone simulation on the microstructure and mechanical behavior of a 2195 aluminium-lithium alloy. Metall Mater Trans A Phys Metall Mater Sci. 2001;32:2729–2741. doi:10.1007/s11661-001-1025-6.
[7] Ma YE, Zhao Z, Liu B, et al. Mechanical properties and fatigue crack growth rates in friction stir welded nugget of 2198-T8 Al-Li alloy joints. Mater Sci Eng A. 2013;569:41–47. doi:10.1016/j.msea.2013.01.044.
[8] Häusler I, Schwarze C, Bilal M, et al. Precipitation of T1 and θ′ phase in Al-4Cu-1Li-0.25Mn during age hardening: microstructural investigation and phase-field simulation. Materials (Basel). 2017;10:117, doi:10.3390/ma10020117.
[9] Wang SC, Starink MJ. Precipitates and intermetallic phases in precipitation hardening Al–Cu–Mg–(Li) based alloys. Int Mater Rev. 2005;50:193–215. doi:10.1179/174328005X14357.
[10] Taylor P, De Geuser F, Malard B. Microstructure mapping of a friction stir welded AA2050 Al – Li – Cu in the T8 state. Philos Mag. 2014;94:37–41. doi:10.1080/14786435.2014.887862.
[11] Qin H, Zhang H, Wu H. The evolution of precipitation and microstructure in friction stir welded 2195-T8 Al-Li alloy. Mater Sci Eng A. 2015;626:322–329. doi:10.1016/j.msea.2014.12.026.
[12] Milagre MX, Mogili NV, Donatus U, et al. On the microstructure characterization of the AA2098-T351 alloy welded by FSW. Mater Charact. 2018;140:233–246. doi:10.1016/j.matchar.2018.04.015.
[13] de S. Araujo JV, de S.C. Milagre C, Xavier Machado M, et al. Estudo da influência dos tratamentos termomecânicos T8 e T851 na microestrutura e na resistência à corrosão da liga AA2198. Corrosão & Proteção. 2018;63:32–44.
[14] Donatus U, Terada M, Ospina CR, et al. On the AA2198-T851 alloy microstructure and its correlation with localized corrosion behaviour. Corros Sci. 2018;131:300–309. doi:10.1016/j.corsci.2017.12.001.
[15] Ma Y, Zhou X, Huang W, et al. Crystallographic defects induced localised corrosion in AA2099-T8 aluminium alloy. Corros Eng Sci Technol. 2015;50:420–424. doi:10.1179/1743278214Y.0000000237.
[16] Ma Y, Zhou X, Liao Y, et al. Localised corrosion in AA 2099-T83 aluminium-lithium alloy: the role of grain orientation. Corros Sci. 2016;107:41–48. doi:10.1016/j.corsci.2016.02.018.
[17] Li JF, Li CX, Peng ZW, et al. Corrosion mechanism associated with T1 and T2 precipitates of Al-Cu-Li alloys in NaCl solution. J Alloys Compd. 2008;460:688–693. doi:10.1016/j.jallcom.2007.06.072.
[18] Victor de Sousa Araujo J, de Fátima Santos Bugarin A, Donatus U, et al. Thermomechanical treatment and corrosion resistance correlation in the AA2198 Al-Cu-Li alloy. Corros Eng Sci Technol. 2019;54:575–586. doi:10.1080/1478422X.2019.1637077.
[19] Milagre MX, Donatus U, Machado CSC, et al. Comparison of the corrosion resistance of an Al–Cu alloy and an Al–Cu–Li alloy. Corros Eng Sci Technol. 2019: 1–11. doi:10.1080/1478422X.2019.1605472.
[20] Lei X, Saatchi A, Ghanbari E, et al. Studies on pitting corrosion of Al-Cu-Li alloys Part I: effect of Li addition by microstructural, electrochemical, in-situ, and pit depth analysis. Materials (Basel). 2019;12:1600–1616. doi:10.3390/ma12121912.
[21] Milagre MX, Donatus U, MacHado CSC, et al. Exfoliation corrosion susceptibility in the zones of friction stir welded AA2098-T351. J Mater Res Technol. 2019;8:5916–5929. doi:10.1016/j.jmrt.2019.09.066.
[22] da Silva RMP, Milagre MX, de Oliveira LA, et al. The local electrochemical behavior of the AA2098-T351 and surface preparation effects investigated by scanning electrochemical microscopy. Surf Interface Anal. 2019;51:982–992. doi:10.1002/sia.6682.
[23] Milagre MX, Donatus U, Mogili NV, et al. Galvanic and asymmetry effects on the local electrochemical behavior of the 2098-T351 alloy welded by friction stir welding. J Mater Sci Technol. 2020;45:162–175. doi:10.1016/j.jmst.2019.11.016.

[24] Xu X, Hao M, Chen J, et al. A influence of microstructural and crystallographic inhomogeneity on tensile anisotropy in thick-section Al–Li–Cu–Mg plates. Mater Sci Eng A. 2022;829:1–11. doi:10.1016/j.msea.2021.142135.

[25] Gable BM, Csontos AA, Starke EA. A quench sensitivity study on the novel Al-Li-Cu-X alloy AF/C 458. J Light Met. 2002;2:65–75. doi:10.1016/S1471-5317(02)00024-X.

[26] Kuo Z, Liu J, Mei YU, et al. Through thickness inhomogeneity of precipitate distribution and pitting corrosion behavior of Al–Li alloy thick plate. Trans Nonferrous Met Soc China. 2019;29:1793–1802.

[27] Crosby KE, Mirshams RA, Pang SS. Development of texture and texture gradient in Al-Cu-Li (2195) thick plate. J Mater Sci. 2000;35:3189–3195.